

# Spontaneous tubulation of membrane vesicles coated with bio-active filaments.

<sup>1</sup> Gaurav Kumar, <sup>2</sup> N. Ramakrishnan, and <sup>1</sup> Anirban Sain\*  
<sup>1</sup> Physics Department, Indian Institute of Technology-Bombay,  
 Powai, Mumbai, 400076, India. <sup>2</sup> Department of Bioengineering,  
 University of Pennsylvania, Philadelphia, PA, 19104, USA

Narrow membrane tubes are commonly pulled out from the surface of phospholipid vesicles using forces applied either through laser or magnetic tweezers or through the action of processive motor proteins. Recent examples have emerged where such tubes spontaneously grow from vesicles coated with bioactive cytoskeletal filaments (e.g. FtsZ, microtubule) in the presence GTP. We show how a soft vesicle deforms due to the interplay between its topology, local curvature and the forces due to the active filaments. We present results from Dynamically Triangulated Monte Carlo simulations of a spherical continuum membrane coated with a nematic field and show how the intrinsic curvature of the filaments and their ordering interactions drive membrane tubulation. We predict interesting patterns of nematic defects, on curved 2D membrane surfaces, which promote tube formation. Implication of our model for more dynamic cases where vesicles coated with an active mixture of microtubule and myosin show shape oscillation, are also discussed. All these cases point to a common theme that defect locations on 2D membrane surfaces are hot spots of membrane deformation activity.

PACS numbers: PACS : 87.16.-b, 87.15.Aa, 81.40.Jj, 87.15.Rn

## INTRODUCTION

Narrow membrane tubes are ubiquitous in eukaryotic cells and are essential for a number of cell functions including signalling and trafficking. Some examples of tubular structures include the axons and dendrites of nerve cells, tubular networks in the Golgi body and the Endoplasmic reticulum. The curvature energy of a tubular protrusion  $E \propto (l/r)$ , where  $l$  is the length of the tube and  $r$  the radius. As a result the formation of narrow tubes (characterised by  $l \gg r$ ) requires extremely high energies and hence they are not expected to be stable unless stabilised by external forces [1]. Membrane tubes are routinely pulled out from vesicles by applying external forces via laser tweezers [2] or suction forces [3]. Tubes have been also pulled out by attaching membrane bound beads to processive molecular motors [4].

Spontaneous tubulation was first reported by Li et. al. [5] in a phase separating mixture confined in a vesicle. The tubes resulted from deflation of the vesicle and were stabilised by spontaneous curvature of the membrane. Here we address a class of experiments where membrane tubes emerge spontaneously due to surface active filamentous proteins, like FtsZ and microtubule, attached to the surface of artificial membrane vesicles (liposomes). Osawa et. al. [6] attached membrane targeted FtsZ filaments onto the outer surface of large GUVs' and observed spontaneous tubulation. Similar tubulation along with interesting periodic dynamics were also recently reported by Keber et. al. [7] who had attempted to bio-mimic cell cortex by assembling arrays of microtubules on the inner wall of a vesicle. Ref [7] and subsequently other groups [8] modelled this microtubule-membrane system as nematics on a spherical surface and studied the effec-

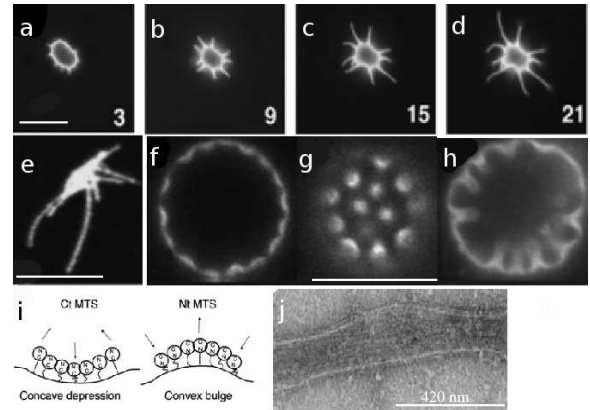


FIG. 1: Growth of tubes from vesicle, shown in (a) to (d), with time shown in minutes. Fluorescent markers are attached to membrane targeted FtsZ filaments. (e) shows loss of spherical shape due to excessive tubulation. (f) and (g) show high resolution images focused at the equatorial plane and the surface, respectively, of the tubulated vesicle. Nearly regular pattern of tubulation sites are visible. (h) shows reverse tubulation i.e., convex bulges on the vesicle surface accompanied by membrane invaginations protruding inward. (i) shows two different ways of anchoring FtsZ onto the membrane, causing opposite membrane curvatures. (j) shows parallel arrangement of FtsZ filaments along the tubular axis. Scale bars are  $10\mu\text{m}$  in the upper and middle rows, and  $420\text{nm}$  in the lower row. Adapted from Fig.1,2,3 and 6 of Ref[6], with permission.

tive dynamics of nematic defects. Charge of a nematic defect is defined as the total amount of rotation a nematic director undergoes as a closed loop is traversed around a defect in the anti-clockwise direction. The defect dynamics becomes interesting because of the Poincare index theorem, which restricts that the total charge of all defects on a sphere must add up to  $+2$ . Furthermore, the

effect of the microtubule or FtsZ filaments on the elastic membrane surface is also very interesting because it leads to nontrivial deformation of the vesicle shape, as seen in Refs [7] and [6], which is the focus of this article. The key objective of our work is to explain FtsZ induced tubulation of vesicle and explore its implications for the microtubule based tubulation process.

In Osawa's experiments [6] FtsZ generated convex (bulge) or concave (depression) on the vesicle surface depending on whether the membrane anchors (FtsA) were attached to the C terminal or the N terminal of the filaments, respectively, as illustrated in Fig. 1(i). Depending on the type of attachment, membrane tubes either grew outward (see the time series in Fig. 1a-d) or inward (see Fig. 1h). While elongation of tubes were observed only when GTP was in abundance, tubes shrunk when medium was depleted of GTP, implying the essential role played by GTP. This is generic of active systems. Furthermore, contrary to expectation, FtsZ filaments with its intrinsic curvature comparable to the tube radius, were found to arrange themselves along the long axis of the tubes rather than arranging in the azimuthal direction, as is common for many other biofilaments e.g., dynamin, ESCRT III [9, 10].

FtsZ filaments are known to have intrinsic curvature of order ( $100\text{--}200\text{ nm}^{-1}$ ) and are known to play important role during cytokinesis of rod shaped bacteria like *E. coli* and *B. subtilis* [11, 12]. In the presence of GTP, FtsZ filaments also condense into bundle via weak ( $< k_B T$ ), lateral inter-filament attraction [13]. These bundles can also locally bend membrane and generate constriction forces (few pico-Newtons) [14] on relatively wide membrane tubes of diameter  $1 - 2\mu\text{m}$ . Given these properties of FtsZ filaments it has remained a puzzle as to how these tubes form. In this article, using an elasticity based model for the lipid membrane that also accounts for filament induced anisotropic membrane curvature [15–17] we show how tubes form from a vesicle and predict the pattern of arrangement of FtsZ filaments on the vesicle. A qualitative hint for corresponding surface pattern is manifest in Fig. 1 which suggests that concave depressions and tubes go hand in hand and that tubes form at the junctions where such concave patches meet. Furthermore we see that the patches are quite regular in arrangement, with coordination number five or six. This is reminiscent of pentagons and hexagons used to tile a sphere.

## MODEL : NEMATICS ON MEMBRANE

We model the FtsZ-membrane system as nematics adhering on a deformable fluid membrane. This model was developed and extensively studied by one of the authors [15–17]. Here, the local orientation of the nematic field is denoted by the unit vector  $\hat{n}(\vec{r})$  which lies in the local

tangent plane of the membrane and is free to rotate in this plane. The filaments induce anisotropic, intrinsic, membrane curvature which can be positive (convex) or negative (concave). Along the bending direction of the FtsZ filament an induced membrane curvature is expected but origin of any intrinsic curvature perpendicular to the filament is not obvious and will be interpreted later. The total energy of the system is

$$E = \int dA \left[ \frac{\kappa_0}{2} (2H)^2 + \frac{\kappa_{\parallel}}{2} (H_{\parallel} - c_{\parallel})^2 + \frac{\kappa_{\perp}}{2} (H_{\perp} - c_{\perp})^2 \right] + \int dA \left[ \frac{K_1}{2} (\tilde{\nabla} \cdot \hat{n})^2 + \frac{K_3}{2} (\tilde{\nabla} \cdot \hat{t})^2 \right]. \quad (1)$$

Here  $\kappa_{\parallel}$  and  $\kappa_{\perp}$  are the induced membrane bending rigidities, while  $\kappa_0$  is the rigidity for the bare membrane.  $2H = c_1 + c_2$  is the mean curvature, where  $c_1, c_2$  are the local principal curvatures on the membrane surface along orthogonal tangent vectors  $\hat{t}_1$  and  $\hat{t}_2$ .  $\hat{n}$  makes an angle  $\phi$  with  $\hat{t}_1$ .  $c_{\parallel}, c_{\perp}$  are the induced intrinsic curvatures along  $\hat{n}$  and  $\hat{t}$ , respectively, where  $\hat{t}$  is perpendicular to  $\hat{n}$ , in the tangent plane.

The curvatures along  $\hat{n}$  and  $\hat{t}$  are given by  $H_{\parallel} = c_1 \cos^2 \phi + c_2 \sin^2 \phi$  and  $H_{\perp} = c_1 \sin^2 \phi + c_2 \cos^2 \phi$ .  $K_1$  and  $K_3$  are the splay and bend elastic constants for the in plane nematic interactions.  $\tilde{\nabla}$  is the covariant derivative on the curved surface.

As in Ref[15], we use a discrete form of this energy functional to perform Monte-Carlo simulation on a triangulated membrane and shapes are explored by moving the vertices (see details in Ref[15]). Each vertex  $i$  hosts a orientation vector  $\hat{n}_i$ . In particular, we use the standard Lebwohl-Lasher model  $E_{nn} = -\epsilon_{LL} \sum_{i>j} (\frac{3}{2}(\hat{n}_i \cdot \hat{n}_j)^2 - \frac{1}{2})$ , [18] to mimic the in plane nematic interaction terms, in the second line of Eq.1, in the one constant approximation ( $K_1 = K_3$ ). While  $\epsilon_{LL}$  is strength of the nematic interaction, the sum  $\sum_{i>j}$  is over all the nearest neighbour ( $i, j$ ) vertices on the triangulated grid, promoting alignment among the neighbouring orientation vectors.

## RESULTS:

Monte-Carlo simulation of our model (Eq.1) shows that, for  $c_{\parallel} < 0, c_{\perp} > 0$ , with  $|c_{\parallel}| \ll |c_{\perp}|$ , regularly spaced narrow tubes emerge (see Fig.2) from an initially spherical vesicle. While  $c_{\perp}$  control the tube radii,  $c_{\parallel}$  sets the inter tube distance. We set  $c_{\parallel} = -0.05, c_{\perp} = 1.0$ , which produce more than 30 tubes (see Fig.2 a,b,c) on an initially spherical liposome of volume  $10^4$  (in arbitrary units). Reversing the signs of the intrinsic curvatures, i.e.,  $c_{\parallel} > 0, c_{\perp} < 0$  tubes grow into the vesicle (see Fig.2 a,d,e). FtsZ coated membrane is expected to be stiffer than the bare bilayer membrane, with isotropic bending rigidity  $\kappa_0 \sim 20k_B T$ . We set  $\kappa_{\parallel} = 35k_B T$  and  $\kappa_{\perp} = 25k_B T$ . We found that setting  $\kappa_0 = 0$  or

$\kappa_0 = 20k_B T$  do not make any difference to the final tubular structures, except that nonzero  $\kappa_0$  offers an initial energy barrier for tube nucleation making tubulation slow, which could be bypassed by raising the temperature temporarily in our Monte-Carlo simulation. We performed simulations separately for fixed volume and fixed area ensembles. We noticed no significant change in the qualitative results in these two different ensembles, except that the simulation with constant area is relatively faster. Experimentally, total fluorescence of the membrane bound FtsZ was found to increase during tubulation [6]. This could be due to addition of higher density of filaments to the tubes from the solution or could be due to release of entropic membrane folds leading to increase in vesicle area.

Note that, all these membrane shapes with growing tubes are transient in nature and the fully tubulated state is the true equilibrium shape. This is consistent with the experimental observation (see Fig1.e for example). In fact Osawa et al [6] observed that tubes shrink when GTP is depleted. In our model this is obtained by turning off  $\kappa_\perp$  to zero which causes the tubes to shrink. It is known that hydrolysis causes FtsZ to adopt a greater intrinsic curvature which we implement by raising  $c_\parallel$  in our model. The reason for turning off  $\kappa_\perp$  will be discussed later.

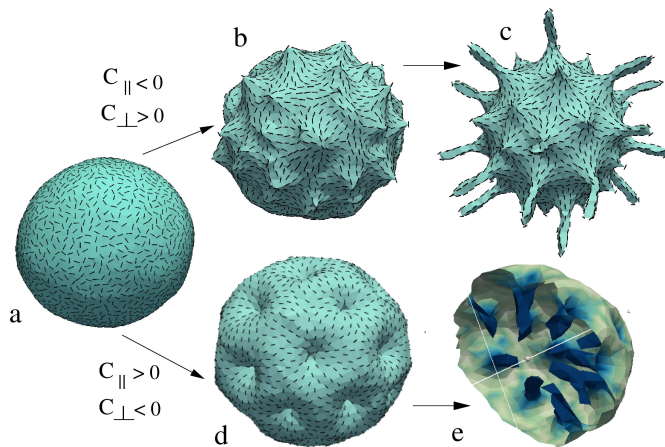


FIG. 2: Growth of tubes, outward or inward, depend on the signs of  $c_\parallel$  and  $c_\perp$ . Here we use  $c_\parallel = -0.05$  and  $c_\perp = 1$  for outward growing tubes, and flip the signs of the intrinsic curvatures, i.e.,  $c_\parallel = 0.05$  and  $c_\perp = -1$  for inward growing tubes. The other parameters are  $\kappa_\parallel = 35$ ,  $\kappa_\perp = 25$  and  $\epsilon_{LL} = 3$ , in units of  $k_B T$ . The volume of the tubulated vesicle is held constant. They are accompanied by concave valleys or convex bulges, respectively, on the vesicle surface. (a,b,c) shows time evolution of outward tubes and (a,d,e) show that of inward tubes. In (e) the vesicle is sectioned to make the inner tubes visible. The inner tubes grow till they start to touch each other due to excluded volume effect. The results from constant area ensemble are nearly identical at same parameter values.

Nematic defects turn out to be hot spots of activity on the membrane. In our simulation tubes emerge from

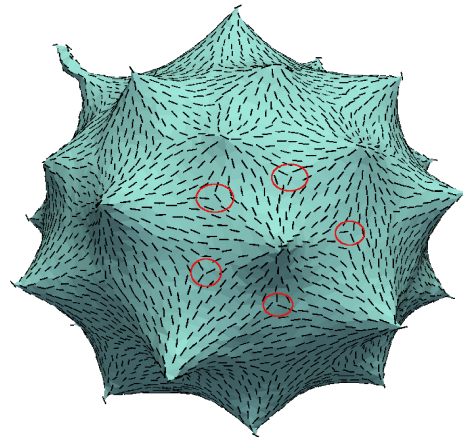


FIG. 3: Arrangement of nematic defects on a tubulating vesicle. The red circles denote  $s = -1/2$  defects which encircle the aster like  $s = +1$  defects. The parameters are same as in Fig-2.

sites of nematic defects with positive defect charge. In Keber et. al. [7] defect sites on ellipsoid shaped vesicle constitute weak spots that encourage growth of MT bundles which in turn induce tubulation. Ladoux's group [19] has shown cell death and extrusion occur at the sites of topological defects in nearly 2D epithelial tissue. It turns out that energetically it is favourable to co-localize nematic defects and high membrane curvature. However arrangement of nematic defects on closed surfaces must obey certain topological theorems. According to Poincare's index theorem (popularly known as the hairy ball theorem) the total charge ( $s$ ) of all the defects on a sphere must add up to 2 (more generally to  $2(1 - g)$  on a surface of genus  $g$ ). This constrains the number and location of the tubes on the vesicle surface. What precedes a tube is a defect of charge  $s = 1$  with aster like arrangement of nematics. The membrane deforms into a pointed structure (vertex) around the aster and produce a tube. Total positive charge increases with number of tubes but this is efficiently nullified by local arrangement of  $s = -1/2$  defects around each tube. Each vertex is surrounded by mainly five or six, and seldom seven, other vertices. Accordingly, the central vertex forms five, six or seven triangles, with the surrounding vertices. Each triangle forms a concave valley and hosts a  $s = -1/2$  defect (red circles in Fig.3). But each  $s = -1/2$  defect is shared by three  $s = 1$  defects. To compute total defect charge on the vesicle, we consider contributions from polygons formed by the  $-1/2$  defects (red circles in Fig.3) The net charge of a pentagon is  $1 + 5 \times (-1/2) \times (1/3) = 1/6$  while that for a hexagon is  $1 + 6 \times (-1/2) \times (1/3) = 0$ , and heptagon is  $-1/6$ . One realisation of this pentagon-hexagon arrangement is the minimal soccer ball structure which has 12 pentagons, 20 hexagons (and therefore

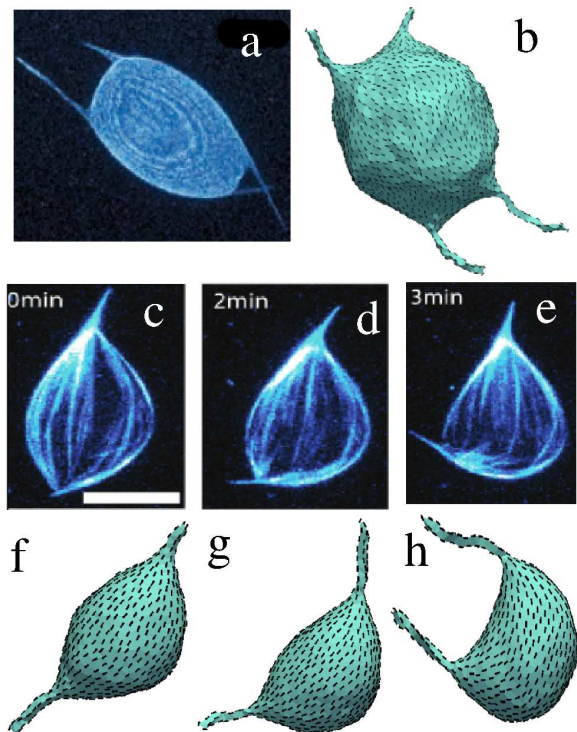


FIG. 4: Exploration of the parameter space at constant volume, for a softer vesicle. In Keber et al [7], upon partial deflation, the vesicle deforms to give rise to four tubes (a). However at a reduced vesicle volume two tubes (c to e) form. The location of the tubes and their lengths oscillate due to active MT dynamics. We reproduce similar shapes (b, and f,g,h respectively), except the oscillations, by studying shapes at  $\kappa = 0, \kappa_{\parallel} = 20, \kappa_{\perp} = 20, c_{\parallel} = -0.01, c_{\perp} = 1.2, \epsilon_{LL} = 9$ . The vesicle volume in (f,g,h) is one third of the volume in (b). In (b) four  $s = -1/2$  defects are generated to compensate for the four  $s = +1$  defects at the tubes but in (f,g,h) no such compensations is needed. b,c,d,e are adapted from Ref [7] (with permission)

thirty-two  $+1$  and sixty  $-1/2$  defects) and thus the total charge adds up to 2. However, smaller and larger vesicles have different number of defects, for example, seventy-six  $-1/2$  and forty  $+1$  defects, still adding up to 2 (in fact Fig.3 has this structure). The regular arrangement of valleys and tubes now can be matched with Fig.1f and -1g, respectively. Note from Fig.3, that each tube ( $+1$  defect) typically has five to six nearest neighbours while each valley ( $-1/2$  defect) has three nearest neighbours.

Once a tube forms it renders stability to the nematic arrangement surrounding the base of the defect. Formation of the high energy  $s = 1$  defects, in our model, is facilitated by the energy gain at the concave valleys (effect of  $c_{\parallel} < 0$ ) and the lateral attraction between filaments, which is effectively promoted via the  $c_{\perp}$  term in Eq.1. By switching off the intrinsic curvature terms we checked that only four low energy  $+1/2$  defects form on non-tubulated vesicle and the defect arrangement fluctu-

ates between the tetrahedral and planar configuration as reported in Keber et al [7]. In our model the filaments cannot slide / translate, unlike in the case of active vesicles in Keber et al [7], however the defects can move due to rearrangement of the nematics.

Though our model does not incorporate the rich dynamics of the active microtubules (MT) present in experiments of Keber et. al. [7], studying our model for appropriate values of  $c_{\parallel}$  and  $c_{\perp}$  turn out to be useful to understand the various dynamical shapes reported in Ref[7]. In particular, we have neither modelled the growing / shrinking MTs, nor their sliding motion, which renders the defects unstable leading to shape oscillations of the vesicles. However, close resemblance of many of our transient shapes to their nonequilibrium counterparts in Ref[7] (see Fig.4) implies that the non-isotropic nature of the equilibrium membrane-nematic free energy still plays an important part in the nonequilibrium dynamics. While in Ref[7] the active MT dynamics controls the position of the defects the tubes still emerge from the defect locations. The same feature is seen in our equilibrium simulation (Fig.4) although the tubes do not oscillate in length and change their position as in Ref[7]. It is known that MT bundles can push out needle like membrane protrusions [20]. Such a protrusion is equivalent to local enhancement of  $c_{\perp}$ . Due to volume conservation this local effect however has a bearing on the global vesicle shape and more so for a smaller volume. The defects and the tubes therefore organise in a specific manner as in Fig4.c and Fig4.d for relatively larger and smaller volume, respectively.

Note that the areal density of nematics can be non-uniform in our model, because although there is one filament per vertex the areal density of vertices is higher on the tubes than in the valleys. This could be very well the case in the experiment. For example, parallel arrangement of filaments on the tubes will produce better coverage and hence higher areal density than that in the valleys. This hikes the relative contribution of the tubes to the overall energy although their area contribution is low. An important revelation from Fig.3 is that the membrane tubes here cannot be considered as axis-symmetric shapes because base of each tube has discrete (5,6 or even 7 fold) rotational symmetry, as the tube is surrounded by discrete number of  $-1/2$  defects.

In summary, we showed how anisotropic curvature induced by FtsZ filaments on phospholipid vesicle gives rise to spontaneous tubulation. Although our model do not incorporate the details of active microtubule dynamics it fares reasonably well in reproducing all the different vesicle shapes obtained in the experiments of Keber et al [7] by invoking effective induced curvatures on the vesicle membrane. The prediction of the filament arrangement on the vesicle surface is an interesting by product of our numerical investigation thanks to the topological properties of closed shapes. So far all theoretical papers in

the context of shape changing vesicles have only considered effective interactions between the so called defect particles, assuming the vesicle shape to be static. Such an approach definitely ignore the many body effect of the nematics that in the first place generate the defects. Furthermore, the interaction between the defects change when the shape of the vesicle changes. We, on the other hand, retain the full many body effects of the nematics and their interactions with the local membrane degrees of freedom. A kinetic MC approach can also generate the full temporal dynamics which we plan to study in future.

GK acknowledges financial support from CSIR (India).

---

\* Electronic address: [asain@phy.iitb.ac.in](mailto:asain@phy.iitb.ac.in)

- [1] I. Derenyi, F. Julicher, and J. Prost . Physical review letters **88**, 238101 (2002)
- [2] F. Hochmuth, J.-Y. Shao, J. Dai, and M. P. Sheetz . Biophysical journal **70**, 358 (1996).
- [3] R. Hochmuth, H. Wiles, E. Evans, and J. McCown . Biophysical journal **39**,83 (1982).
- [4] A. Roux, G. Cappello, J. Cartaud, J. Prost, B. Goud and P. Bassereau . Proceedings of the National Academy of Sciences **99**,5394 (2002).
- [5] Y. Li, R. Lipowsky, and R. Dimova. Proceedings of the National Academy of Sciences **108** ,4731 (2011).
- [6] M. Osawa, D. E. Anderson, and H. P. Erickson. The EMBO journal **28**,3476 (2009).
- [7] F. C. Keber, E. Loiseau, T. Sanchez, S. J. DeCamp, L. Giomi, M. J. Bowick, M. C. Marchetti, Z. Dogic, and A. R. Bausch. Science **345** ,1135 (2014).
- [8] F. Alaimo, C. Kohler, and A. Voigt. arXiv preprint arXiv:1703.03707 (2017).
- [9] H. H. Low, C. Sachse, L. A. Amos, and J. Lowe. Cell **139** ,342 (2009).
- [10] A. Y. Adell, D. Teis, et al. FEBS letters **585** ,3191 (2011).
- [11] X. Yang, Z. Lyu, A. Miguel, R. McQuillen, K. C. Huang and J. Xiao. Science **355** ,744 (2017).
- [12] A. W. Bisson-Filho, Y.-P. Hsu, G. R. Squyres, E. Kuru, F. Wu, C. Jukes, Y. Sun, C. Dekker, S. Holden, M. S. VanNieuwenhze, et al.. Science **355**,739 (2017).
- [13] B. Ghosh and A. Sain. Physical review letters **101**,178101 (2008).
- [14] M. Osawa, D. E. Anderson, and H. P. Erickson. Science **320** ,792 (2008).
- [15] N. Ramakrishnan, P. S. Kumar, and J. H. Ipsen. Physical Review E **81**,041922 (2010).
- [16] N. Ramakrishnan, P. S. Kumar, and J. H. Ipsen. Biophysical journal **104** ,1018 (2013).
- [17] N. Ramakrishnan, P. S. Kumar, and J. H. Ipsen. Macromolecular Theory and Simulations **20** ,446 (2011).
- [18] P. Lebwohl. Phys. Rev. A **6** ,426 (1972).
- [19] T. B. Saw, A. Doostmohammadi, V. Nier, L. Kocgozlu, S. Thampi, Y. Toyama, P. Marcq, C. T. Lim, J. M. Yeomans, and B. Ladoux. Nature **544** ,212 (2017).
- [20] D. K. Fygenson, J. F. Marko, and A. Libchaber. Physical review letters **79**,4497 (1997).